JOURNAL OF MATERIALS SCIENCE 29 (1994) 1127–1134

The Young's moduli of *in situ* Ti/TiB composites obtained by rapid solidification processing

Z. FAN, A. P. MIODOWNIK
Department of Materials Science and Engineering, University of Surrey, Guildford, Surrey GU2 5XH, UK

L. CHANDRASEKARAN, M. WARD-CLOSE
Materials and Structures Department, Defence Research Agency, Farnborough, Hampshire GU14 6TD, UK

In situ Ti/TiB composites (Ti–6Al–4V matrix reinforced with TiB phase) with different volume fractions of the TiB phase, have been produced by consolidation of rapidly solidified Ti–6Al–4V alloys with different levels of boron addition. The microstructural examination of such composites shows that the reinforcing phase has a fine grain size and a uniform distribution throughout the matrix. The Young's moduli of the *in situ* composites have been determined experimentally to study the strengthening effect of the TiB phase. It was found that the Young's modulus of an *in situ* composite with 10 vol% TiB phase can be increased to 140 GPa, compared to 116.7 GPa for the matrix alloy. The theoretical predictions are in good agreement with the present experimental results and other results of similar composites obtained by the reactive sintering technique.

1. Introduction

Metal matrix composites (MMCs) have been investigated since the early 1960s [1, 2] with the original aim being the production of materials engineered for specific applications, without much consideration of their cost. However, after more than 20 years of development, MMCs must now also be cost-competitive with other materials. Thus the emphasis of research in MMCs is now towards novel processing techniques, cheaper reinforcement and net or near-net shape production techniques [3, 4]. In addition, it has also been realized that the majority of likely engineering applications will exploit their excellent stiffness rather than the high ultimate tensile strength [5].

Until now, the available techniques for MMC fabrication included (i) diffusion bonding of thin sheets interleaved with ceramic fibres [6–8], (ii) mechanical processing of ceramic suspensions of metallic powders in molten metal ("compocasting") [9, 10], (iii) premixing and consolidation of the metallic powders and ceramic whiskers, fibres and particles [11, 12], (iv) melt infiltration into a preform consisting an assembly of ceramic fibres [13–15], (v) spray codeposition of metal droplets and ceramic particles [16–19] and (vi) *in situ* growth MMCs from molten alloys [20]. The main concerns in the first five processing techniques are the following two recurrent problems: nearly all the commercially significant reinforcements are poorly wetted by molten aluminium, titanium, and their alloys, and several significant reinforcements react with molten aluminium and titanium. The art and science of fabrication of MMCs mainly consist of overcoming these two problems [3, 4]. From a processing point of view, the advantages of *in situ* processing compared with the conventional powder metallurgy and casting particulate approaches include (i) cost-effectiveness, (ii) homogeneous distribution of reinforcement, (iii) finer particles, (iv) improved wettability between reinforcement and matrix, and (v) elimination of the deleterious interface reaction.

Rapid solidification (RS) processing can provide a novel route for fabrication of MMCs, especially for systems in which the reinforcement react strongly with the matrix during their fabrication process, for instance, SiC- or boride-reinforced titanium alloy matrix. Rapid solidification of liquid alloys at a cooling rate greater than $10^4\,K\,s^{-1}$ results in significant undercooling of the melts and leads to several metastable effects which have been broadly divided into constitutional and microstructural effects [21]. For instance, RS allows large departures from equilibrium constitution and results in a large extension of solid solubility. The equilibrium solid solubility of boron in both α- and β-titanium is less than 1 at %. By applying RS, this solubility can be extended beyond 10 at % [22]. This advantage of RS processing over conventional ingot metallurgy can offer us an effective way of producing titanium solid solution with supersaturated boron in it. Upon subsequent heat treatment of the RS product, ceramic phase(s) (in this case TiB) will nucleate within the titanium matrix to form a fine and uniform distribution of ceramic reinforcement [23].

In this paper, the results from an experimental investigation of Young's moduli of *in situ* Ti/TiB

0022–2461

composites produced by rapid solidification processing will be presented and discussed. The approach to Young's modulus of two-phase composites developed by Fan *et al.* [24] will be applied to *in situ* Ti/TiB composites to predict their Young's moduli. The theoretical predictions will be compared with the experimental results.

2. Experimental procedure

2.1. The composite design

Ti–6Al–4V (alloy compositions in weight per cent) is a widely used commercial alloy, and has been extensively studied in the past [25]. Thus there is a better understanding of microstructural evolution and the response of mechanical properties to the microstructural changes in this alloy. Therefore, Ti–6Al–4V has been chosen here as the matrix alloy for fabrication of *in situ* Ti/TiB MMCs. The calculated vertical section at constant aluminium (6 wt %) and vanadium (4 wt %) contents for the Ti–Al–V–B system [26] is presented in Fig. 1. The predicted α/β transus is 935 °C for pure Ti–6Al–4V alloy without boron addition [26], which is in good agreement with the experimental result (937 °C) of Kahveci and Welsch [27]. The predicted eutectic reaction temperature ($L \rightarrow \beta(Ti) + TiB$) for Ti–6Al–4V–XB alloys is 1597 °C, and the eutectic composition for the liquid phase is 1.58 wt % B. Fig. 2 shows the Ti–B binary phase diagram reported by Murray [28], in which the eutectic reaction takes place at 1.6 wt % B, 1540 °C. A comparison between Figs 1 and 2 indicates that the addition of α- and β-stabilisers does not significantly change the stability of the TiB phase, owing to the low solubility of boron in both α- and β-Ti. The boron contents chosen for the composite production are 0.1, 0.2, 0.5, 0.8, 1.5 and 2.0 wt % B. The alloys with less than 1.5 wt % are hyper-eutectic alloys, Ti–6Al–4V–1.5B is a near eutectic alloy and Ti–6Al–4V–2B is a hypo-eutectic alloy.

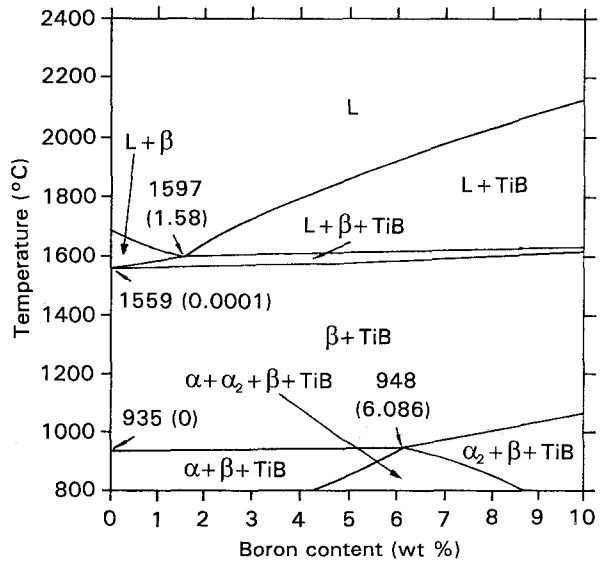

Figure 1 Calculated vertical section of the Ti–Al–V–B quaternary phase diagram at constant aluminium (6 wt %) and vanadium (4 wt %) concentration [26].

2.2. Melting and melt-spinning

Melting and melt-spinning of all the alloys designed for this project were performed in a Marko's advanced melt spinner (Model 5T), which is schematically illustrated in Fig. 3. Melting and melt-spinning was carried out in a stainless steel chamber with a high vacuum/inert gas atmosphere. The alloy was melted in a water-cooled copper hearth using a non-consumable tungsten electrode under a high-purity argon atmosphere. The melt was then delivered at a controlled rate to contact the circumferential surface of a rotating molybdenum wheel by which the melt is rapidly solidified as long fibres with a crescent-shaped cross-section, typically 100–300 μm wide and 40–100 μm thick. The operating parameters used in this work were as follows: the wheel speed was 2500 r.p.m., the gap between the V-notch on the copper hearth and the tip of the molybdenum wheel was about 1.5 mm.

The alloys containing boron were produced by melting together Ti–6Al–4V ingots (containing 0.205 wt % oxygen) and TiB_2 powder (99.5% purity, Johnson Matthey Ltd) wrapped in 0.025 mm thick 99.6% pure titanium foil. To ensure the chemical homogeneity of the melted alloy, the ingots were melted at least three times before final melt spinning. Each melting and melt-spinning operation was conducted after evacuation to at least 10^{-5} torr followed by two flushes of the chamber with high-purity argon.

2.3. Consolidation

To facilitate the consolidation process and ensure the chemical and microstructural homogeneity of the consolidated products, the melt-spun fibres were comminuted into finer particles with particle size less than 200 μm. The comminution process was performed in a glove box which allows the milling operation to be conducted in an argon atmosphere, thereby avoiding the possibility of spontaneous combustion and any further oxygen pick-up by the alloys. The comminuted alloy powders were then filled into cylindrical titanium alloy cans which had a hole drilled into their lids. The lids were first electron welded leaving the hole open. These cans were then baked in the temperature range 250–300 °C in vacuum (10^{-5} torr) before the holes were sealed by electron-beam welding. This procedure was adopted to remove occluded gases in the powder compacts. They were then loaded into a high-temperature isostatic presser (Hiper). The consolidation of different rapidly solidified titanium-alloys was carried out at 900–920 °C, 150–300 MPa for 2 h. Some of the consolidated alloys were then subjected to a further 40% reduction in cross-section by hot pressing (forging) the can at 900 °C to produce a flat piece. In all cases, a fully densified material was achieved, and porosity was rarely observed.

2.4. Mechanical testing

Tensile test pieces were milled from the consolidated and forged material. The final test piece was a thin sheet with a thickness of approximately 1.5–2.5 mm and a gauge length of 14–16 mm. The other dimensions are illustrated in Fig. 4. All the tensile tests were

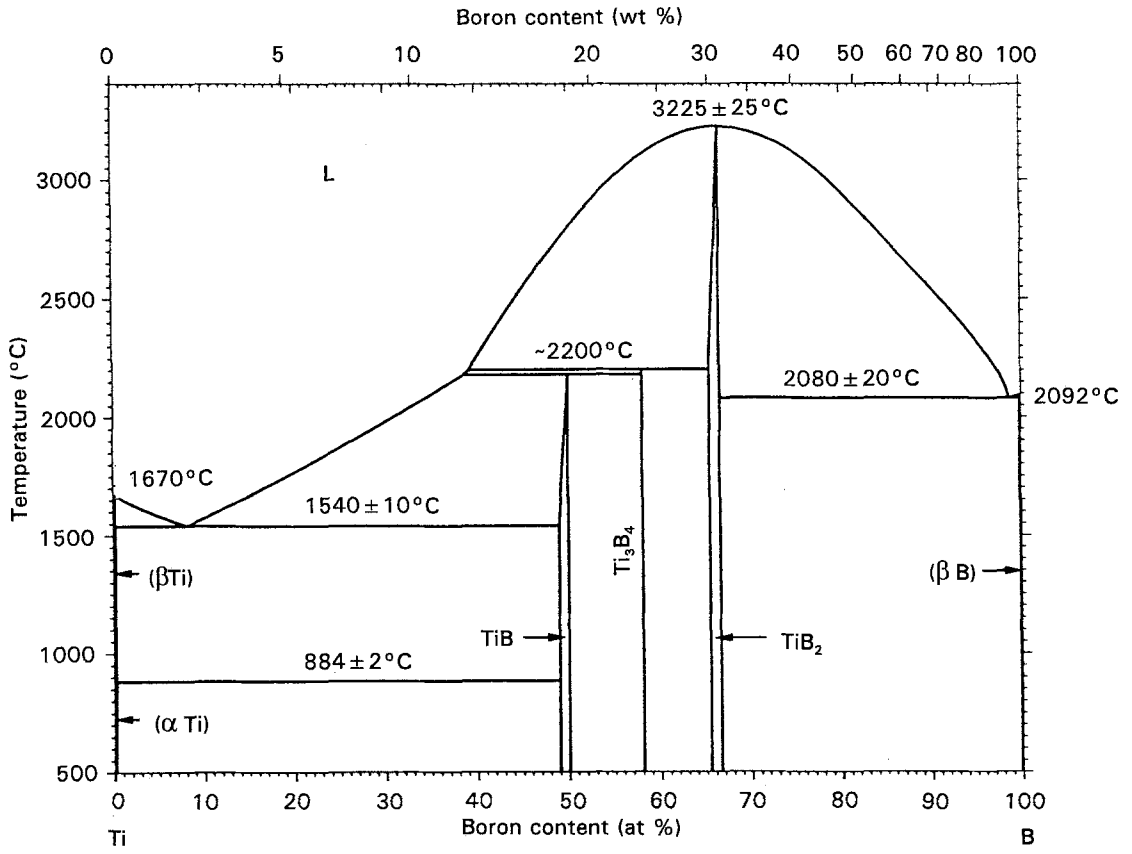

Figure 2 The binary Ti–B phase diagram [28].

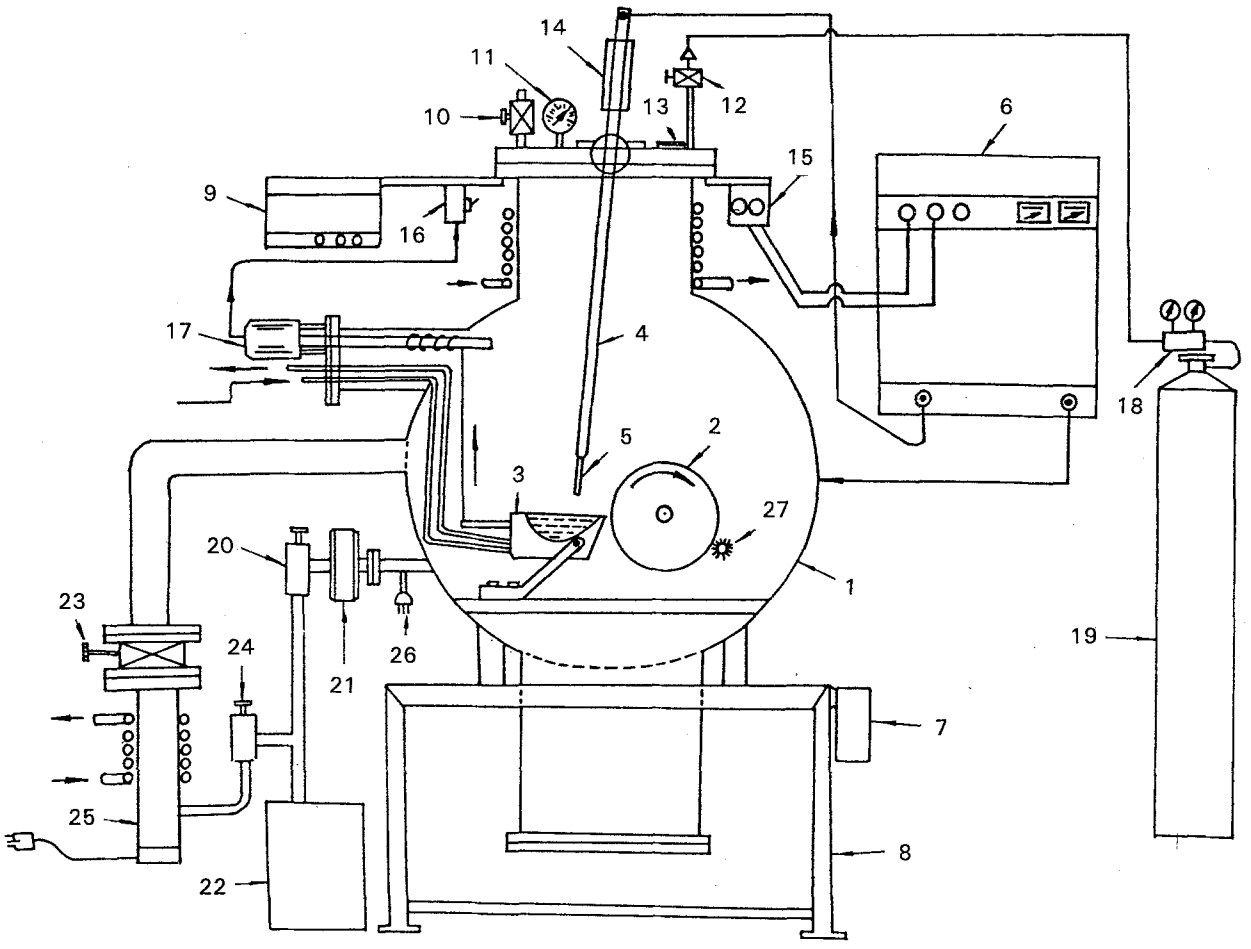

Figure 3 Schematic diagram of the Marko 5T melt-spinner. The arrows in this diagram indicate the water in and out directions. 1, Stainless steel vacuum chamber; 2, rotating casting wheel; 3, water-cooled copper hearth; 4, copper electrode holder; 5, tungsten electrode; 6, d.c. power generator; 7, ionization gauge control; 8, heavy duty steel stand; 9, variable speed drive; 10, air inlet valve; 11, sub-atmospheric pressure gauge; 12, argon inlet valve; 13, quartz view point; 14, nylon handle; 15, power stat for d.c. power generator; 16, switch for tilting motor; 17, tilting motor; 18, two-stage gas regulator; 19, argon tank; 20, mechanical vacuum valve; 21, filter; 22, mechanical pump; 23, gate valve; 24, foreline valve; 25, diffusion pump; 26, thermocouple gauge; 27, brush.

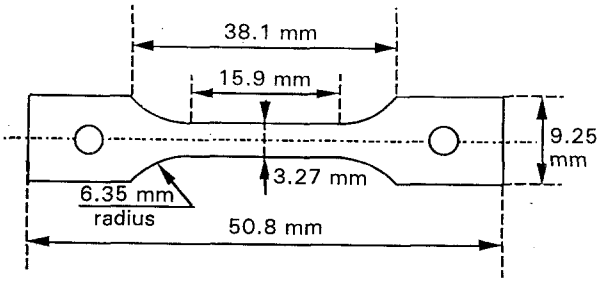

Figure 4 Schematic drawing of the thin sheet test piece used for tensile testing.

performed on a Mayes 100 kN Servo-Hydraulic Uniaxial Tensile/Fatigue Testing Machine fitted with hydraulic grips. The strain rate used was $10^{-3}\,s^{-1}$. Load–elongation curves were obtained on an X–Y plotting table which was linked to the load cell of the machine and to an extensometer clamped to the test piece. The Young's moduli were determined by measuring the slope of the true stress–true strain curve in the elastic range.

2.5. Microstructural examination

Samples for optical microscopy (OM) and scanning electron microscopy (SEM) were taken from the products at different stages of processing, and then cut into suitable shapes before being mounted in conductive bakelite. The mounted samples were polished by applying a conventional polishing technique. The polished specimens were chemically etched by using Kroll's reagent. A Zeiss optical microscope and a Cambridge 250 SEM were used to examine the microstructure of these samples. Specimens for transmission electron microscopy (TEM) were prepared by in a "TENUPOL" unit using an electrolyte of 5 vol % perchloric acid in methanol. The polishing temperature was − 40 °C, the voltage 30 V, the current about 30 mA. The TEM observation was performed on a Jeol 200 CX STEM under an accelerating voltage of 200 kV.

3. Results and discussion

3.1. Microstructure

Owing to the very low solid solubility of boron in both the α- and β-Ti, the TiB phase in the B-containing alloys produced by the traditional ingot metallurgy is usually large and has a non-uniform distribution in the matrix alloy. Fig. 5 shows the microstructure of Ti–6Al–4V–2B alloy ingot solidified in the water-cooled copper hearth. The TiB phase has two distinguished morphologies, the blocky primary TiB and the needle-shaped eutectic TiB, as indicated in Fig. 5. The TiB phase can be greatly refined by rapid solidification processing. This effect of RS processing is demonstrated in Fig. 6 by the microstructure of rapidly solidified Ti–6Al–4V–0.5B and Ti–6Al–4V–2B alloys. The cross-section of rapidly solidified fibres exhibits a two-zone microstructure: the columnar grain zone at the wheel side and the equiaxed dendrite zone at the free side, as indicated in Fig. 6a. This two-

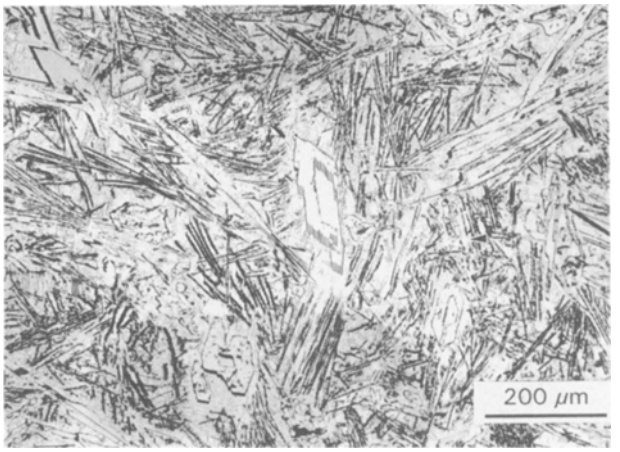

Figure 5 Optical micrograph showing the microstructure of Ti–6Al–4V–2B ingot solidified in the water-cooled copper hearth. The primary TiB has a blocky shape and the eutectic TiB has a needle-shaped morphology.

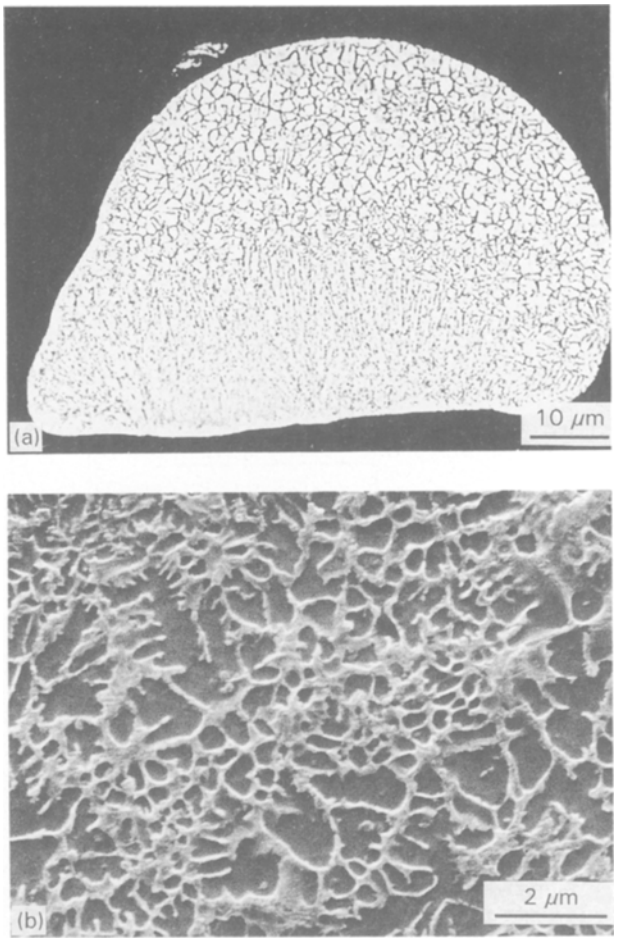

Figure 6 SEM images of the cross-section of the melt-spun fibres. (a) Back-scattered electron image of Ti–6Al–4V–0.5B fibre, with the free side at the top and the wheel side below. (b) secondary electron image of Ti–6Al–4V–0.5B fibre at the free side.

zone microstructure is typical of the melt-spun titanium alloys containing boron [21]. Fig. 6 also shows that there is a boron-concentrated region between the primary α-grains. The detailed TEM work revealed that this region has a eutectic structure (β + TiB) [29].

The microstructures of consolidated Ti–6Al–4V alloys with different amounts of boron addition are shown in Figs 7 and 8. All the borides present in the consolidated specimens were identified as TiB by both X-ray diffraction and electron diffraction techniques [29]. There is no evidence for the existence of the TiB_2 phase in all the consolidated samples with the boron concentration investigated here. After consolidation, the TiB phase has a very fine grain size and a very uniform distribution throughout the Ti–6Al–4V matrix, and exhibits two morphologies: the near-equiaxed TiB and the needle-shaped TiB, as shown by the TEM micrograph of consolidated Ti–6Al–4V–0.8B alloy in Fig. 9. However, different from the TiB phase in the alloy ingot (see Fig. 5), the near-equiaxed TiB particles are formed from the boron-saturated solid solution by a solid-state reaction, and the needle-shaped TiB particles are formed from the eutectic structure (β + TiB) present in the as-quenched state (see Fig. 6) [29]. It is also found that there is a good bonding between the TiB particles and the matrix, and that the TiB/matrix interfaces are sharp with no visible evidence of the presence of any chemical reaction zone as shown by the BF image in Fig. 10.

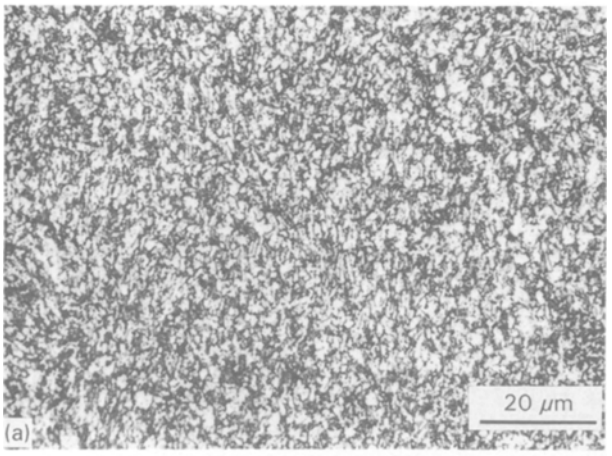

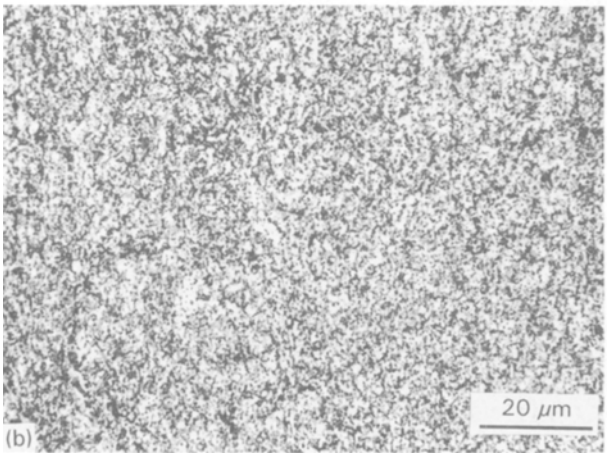

Figure 7 Optical micrographs showing the microstructure of the boron-containing titanium alloys after consolidation at a temperature of 900 °C and a pressure of 250 MPa for 2 h and then forged at 900 °C to 40% reduction in cross-section. (a) Ti–6Al–4V–0.5B, (b) Ti–6Al–4V–0.8B.

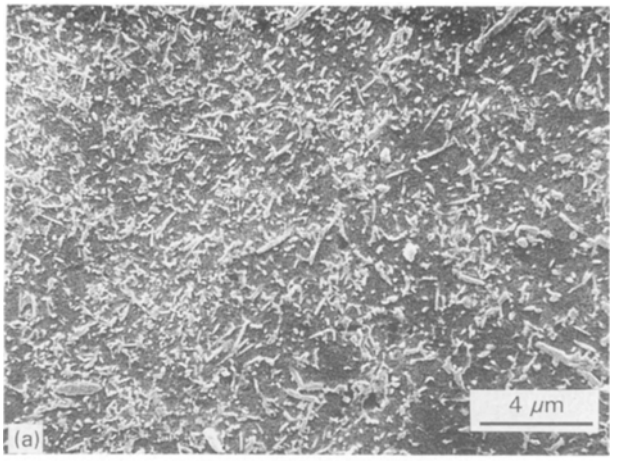

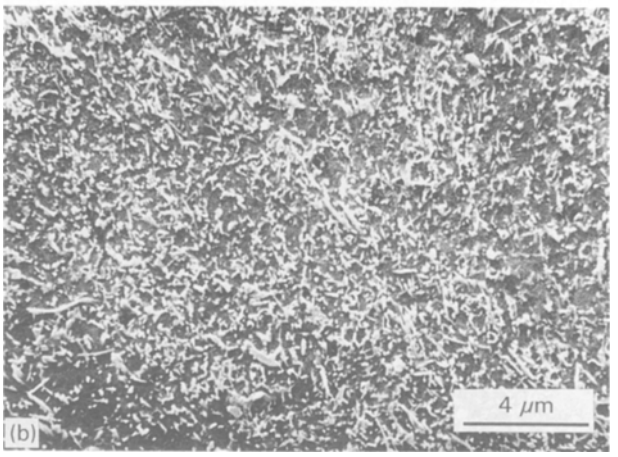

Figure 8 Scanning electron micrographs showing the microstructure of the boron-containing titanium alloys after consolidation at a temperature of 900 °C and a pressure of 250 MPa for 2 h and then forged at 900 °C to 40% reduction in cross-section. (a) Ti–6Al–4V–1.5B, (b) Ti–6Al–4V–2.0B.

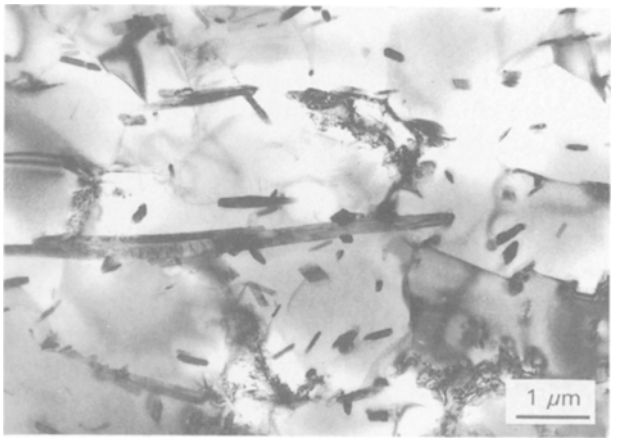

Figure 9 Bright-field TEM images of Ti–6Al–4V–0.8B alloy after consolidation at a temperature of 900 °C and a pressure of 300 MPa for 2 h showing the uniform distribution of nearly equiaxed and needle-shaped TiB particles in the α ($-$ β) matrix.

3.2. Young's modulus of *in situ* Ti/TiB composites

The obtained Young's moduli of *in situ* Ti/TiB composites with different thermomechanical processes are tabulated in Table I. The volume fractions listed in

TABLE I Summary of the Young's moduli of *in situ* Ti/TiB composites

Alloy (wt %)	Expected TiB (vol %)	Processing conditions	*E* (GPa)
Ti–6Al–4V	0.0	HIPed at 900 °C, 300 MPa, 2 h	116.6
Ti–6Al–4V–0.1B	0.5	HIPed at 900 °C, 250 MPa, 2 h and forged at 900 °C	116.2
Ti–6Al–4V–0.2B	1.0	HIPed at 900 °C, 250 MPa, 2 h and forged at 900 °C	121.0
Ti–6Al–4V–0.5B	2.4	HIPed at 900 °C, 250 MPa, 2 h and forged at 900 °C	129.7
Ti–6Al–4V–0.8B	3.9	HIPed at 925 °C, 150 MPa, 2 h	123.5
Ti–6Al–4V–0.8B	3.9	HIPed at 900 °C, 250 MPa, 2 h and forged at 900 °C	128.2
			131.8
Ti–6Al–4V–1.5B	7.1	HIPed at 900 °C, 300 MPa, 2 h	128.6
			132.90
Ti–6Al–4V–1.5B	7.1	HIPed at 900 °C, 250 MPa, 2 h and forged at 900 °C	133,6
			132.0
Ti–6Al–4V–2.0B	9.9	HIPed at 900 °C, 250 MPa, 2 h and forged at 900 °C	139.4
			136.6

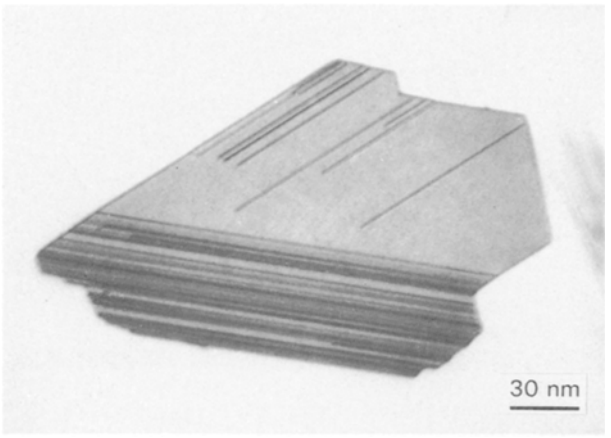

Figure 10 Bright-field TEM image of a near-equiaxed TiB particle in consolidated Ti–6Al–4V–0.8B alloy showing that there is no chemical reaction at the TiB/matrix interface.

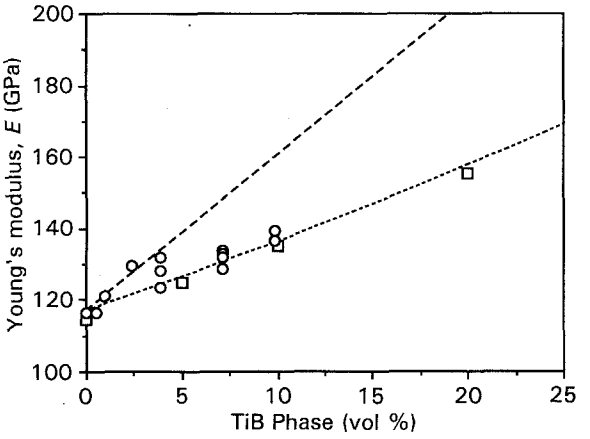

Figure 11 The experimentally measured Young's moduli of *in situ* Ti/TiB composites obtained by rapid solidification processing as a function of the volume fraction of the TiB phase (○). Also shown here are the experimental results of Saito and Furuta [32] for Ti/TiB composites obtained by reaction sintering (□). (– – –) The theoretical predictions of Fan *et al.* [24], (— — —) the prediction by the linear law of mixtures.

Table I are not measured experimentally, due to the extremely fine grain size of the TiB phase, they are calculated from the amount of boron added to the alloy and the densities of the TiB phase (5.26 g cm^{-3} [30] and the matrix (4.45 g cm^{-3} [31]). The Young's moduli of *in situ* Ti/TiB composites listed in Table I are plotted in Fig. 11 as a function of the volume fraction of the TiB phase. Also presented in Fig. 11 are Saito and Furuta's [32] experimental results of Young's moduli of *in situ* Ti/TiB composites obtained by reaction sintering. Qualitatively, there is a good agreement between the experimental results from this investigation and from Saito and Furuta [32]. The scattering of Young's moduli from this investigation is obvious; this is caused by the inherent inaccuracy of measuring Young's moduli from the true stress–true strain curve. However, the strengthening effect of the TiB phase to the Ti–6Al–4V matrix is quite straight foreword. The Young's moduli of *in situ* Ti/TiB composites increases almost linearly with increasing volume fraction of the TiB phase. For instance, the composite's Young's modulus can be increased by 20% (to 140 GPa) from the Young's modulus of Ti–6Al–4V matrix alloy (116.7 GPa) when the volume fraction of the TiB phase reaches 0.1. Therefore, it is desirable to increase the volume fraction of the TiB phase to 0.2–0.3 for further increase of the stiffness of the composite.

3.3. Prediction of the Young's modulus of the *in situ* Ti/TiB composites

In a recent paper, Fan *et al.* [24] developed a new approach for predicting the Young's moduli of two-phase composites based on the topological transformation [29, 33] and the mean-field theory [34, 35]. According to this approach, the Young's modulus of an α–β two-phase composite, E^c, can be expressed in terms of the Young's moduli of the constituent phases and the topological parameters [29, 33] by the following equation

$$E^c = E^\alpha f_{\alpha c} + E^\beta f_{\beta c} + E^{III} F_s \quad (1)$$

where E^α and E^β are the Young's moduli of the α- and β-phases, which can be determined from tests of single-phase specimens, $f_{\alpha c}$ and $f_{\beta c}$ are continuous volumes of the α- and β-phases, and F_s is the degree of

separation [29, 33]. E^{III} is the Young's modulus of the EIII body and can be calculated from the following equation

$$E^{III} = 2G^{III}(1 + \nu^{III}) \quad (2)$$

where G^{III} and ν^{III} are the shear modulus and Poisson's ratio of the EIII body, and G^{III} can be calculated theoretically by applying the mean-field theory [34, 35]

$$G^{III} = \frac{G^{\alpha}}{1 + [f_{\beta III}D/(1 - f_{\beta III}\gamma D)]} \quad (3)$$

where D and γ are defined as

$$D = \frac{G^{\alpha} - G^{\beta}}{(G^{\beta} - G^{\alpha})(1 - \gamma) + G^{\alpha}} \quad (4)$$

$$\gamma = \frac{7 - 5\nu^{\alpha}}{15(1 - \nu^{\alpha})} \quad (5)$$

where G^{α} and G^{β} are the shear moduli of the α- and β-phases, $f_{\alpha III}$ and $f_{\beta III}$ are the volume fractions of the α- and β-phases in the EIII body, and γ is the strain accommodation tensor for spheres. It is assumed that ν^{III} follows the linear law of mixtures, i.e.

$$\nu^{III} = \nu^{\alpha}f_{\alpha III} + \nu^{\beta}f_{\beta III} \quad (6)$$

where ν^{α} and ν^{β} are the Poisson's ratio of the α- and β-phases. It has been shown that the predictions by this approach are in good agreement with the experimental results in the various two-phase composites [24].

The Young's modulus of the monoboride phase (TiB) is not available in the literature. However, the Young's modulus of TiB_2 has been theoretically determined (550 GPa) by applying a thermodynamic approach developed by Miodownik [36]. For the present calculation, it is assumed that $E_{TiB} = E_{TiB_2}$. The Poisson's ratio of the TiB phase (0.14) was adopted from the ZrB_2 phase [37]. For the matrix alloy, the Young's modulus of the matrix is from the experimental results listed in Table I. Poisson's ratio of the matrix is chosen as 0.27, which is the Poisson's ratio of the α-phase [31], because the low volume fraction of the β-phase in the matrix (approximately 0.02–0.05). These parameters are tabulated in Table II.

Because of the extremely fine size of the TiB phase, it is difficult to determine experimentally the topological parameters required for the calculation. However, we can follow the similar assumption made in [24] for other composite systems with a near-random microstructure, i.e.

$$f_{TiBc} = f_{TiB}^4 \quad (7)$$

$$f_{Mc} = f_M^3 \quad (8)$$

TABLE II List of the parameters used for predictions of Young's moduli of *in situ* Ti/TiB composites

Phase	E (GPa)	ν	Remarks
Matrix (Ti–6Al–4V)	116.7	0.27	From [31]
TiB	550 [36]	0.14 [37]	Adopted from ZrB_2

where f_{TiBc} and f_{Mc} are the continuous volume of TiB and the matrix phases, respectively. The calculated Young's moduli of the *in situ* Ti/TiB composites are shown in Fig. 11 and compared with the experimental results from this investigation and from Saito and Furuta [32] by reaction sintering. The predictions by the linear law of mixtures are also presented in this figure for comparison. Fig. 11 shows that the theoretical predictions are in fairly good agreement with the experimental results and superior to the predictions by the linear law of mixtures. Fig. 12 shows the predicted Young's moduli of *in situ* Ti/TiB composites in the complete volume fraction range. Also shown in Fig. 12 are the predictions by the linear law of mixtures for comparison. If the volume fraction of the TiB phase can be increased to 0.2, the predicted Young's modulus will be 158 GPa, i.e. a 35% increase over the unreinforced Ti–6Al–4V matrix.

4. Conclusion

A series of *in situ* Ti/TiB composites (Ti–6Al–4V matrix reinforced with TiB-phase) have been produced by consolidation of rapidly solidified Ti–6Al–4V alloys with different levels of boron addition. The microstructural examination of such composites shows that the reinforcing phase has a fine grain size and a uniform distribution throughout the matrix. There is a good bonding between the TiB particles and the Ti–6Al–4V matrix, and there is no evidence for any chemical reaction at the TiB/matrix interface. The Young's moduli of those *in situ* composites have been determined experimentally to study the strengthening effect of the TiB phase. It was found that the Young's modulus of an *in situ* composite with 10 vol % TiB phase can be increased to 140 GPa from the 116.7 GPa of the matrix alloy. A theoretical approach to the Young's moduli of two-phase composites has been applied to predict the Young's moduli of the *in situ* produced Ti/TiB composites. It is demonstrated that the theoretical predictions are in good agreement with the present experimental results

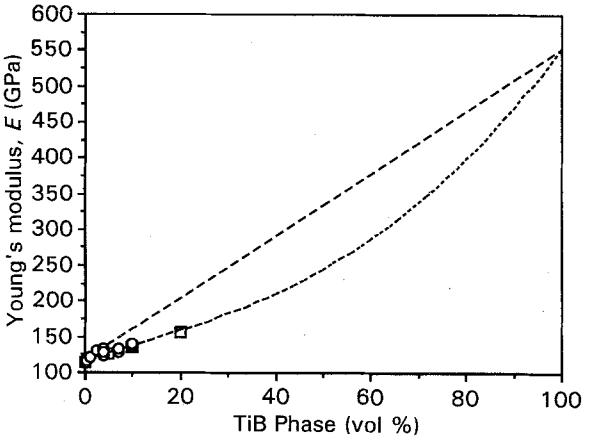

Figure 12 The theoretical predictions of Young's modulus of *in situ* Ti/TiB composites by the approach developed by Fan *et al.* [24] (– – –) in the complete volume fraction range in comparison with the predictions by the law of mixtures (— — —). (○) Experimental values, this work; (□) experimental values. [32].

and the other results in similar composites obtained by the reactive sintering technique.

Acknowledgements

The authors thank Dr P. Tsikiropoulos for useful discussions. This work has been supported by the Ministry of Defence, UK.

References

1. A. KELLY and G. J. DAVIES *Met. Rev.* **10** (1965) 1.
2. D. CRATCHLEY, *ibid.* **10** (1965) 79.
3. A. MORTENSEN and I. JIN, *Int. Met. Rev.* **37** (1991) 122.
4. A. MORTENSEN, J. A. CORNIE and M. C. FLEMINGS, *J. Metals* February **40** (1988) 12.
5. P. J. WITHERS, PhD thesis, University of Cambridge (1988).
6. P. R. SMITH and F. H. FROES, *J. Metals* March **36** (1984) 19.
7. C. G. RHODES, in "Titanium Science and Technology", Vol. 3, edited by G. Lutjering *et al.* Deutsche Gesellschaft Fur Metallkunde, Oberursel (1985) p. 2209.
8. C. G. RHODES and R. A. SPURLING, in "Recent Advances in Composites in USA and Japan", ASTM STP 864, edited by J. R. Vinson and M. Yaya (American Society for Testing and Materials, Philadelphia, PA, 1985) p. 585.
9. C. G. LEVI, G. J. ABBASCHIAN and R. MEHRABIAN, *Met. Trans.* **9A** (1978) 697.
10. B. F. QUIGLEY, G. J. ABBASCHIAN, R. WUNDERLIN and R. MEHRABIAN, *ibid.* **13A** (1982) 93.
11. A. P. DIVECHA, S. G. FISHMAN and S. D. BARMACHA, *J. Metals* September **33** (1981) 12.
12. F. H. FROES and J. R. PICKENS, *ibid.* January **36** (1984) 14.
13. T. W. CLYNE and M. G. BADER in "Proceedings of ICCM-V", edited by W. C. Harrigan, J. Strife and A. K. Dhingra (TMS-AIME, Warrendale, PA, 1985) p. 755.
14. J. A. CORNIE, A. MORTERSEN, M. A. GUNGOR and M. C. FLEMINGS, *ibid.* p. 809.
15. T. W. CLYNE and J. F. MASON, *Met. Trans.* **18A** (1987) 1519.
16. T. NAMAI, Y. OSAWA and M. KIKUCHI, IMONO, *J. Jpn Foundrymen's Soc.* **56** (1984) 604.
17. T. C. WILLIS, J. WHITE, R. M. JORDAN and I. R. HUGHES, in "Solidification Processing 1987" (Institute of Metals, London, 1988) p. 476.
18. Y. TSUNEKAWA, M. OKUMIYA, I. NIMI and K. OKAMURA *J. Mater. Sci. Lett.* **6** (1987) 191.
19. M. R. JACKSON and R. L. MEHAN, in "Proceedings of ICCM-VI", edited by N. C. R. Buskell, J. M. Hodginson and J. Morton (Elsevier, Applied Science, London, 1987) p. 2431.
20. M. J. KOCZAK and K. S. KURMAR, US Pat. 4808372 (1989).
21. C. SURYANARAYANA and F. H. FROES, *Int. Met. Rev.* **36** (1991) 85.
22. S. H. WHANG, *J. Met. Sci.* **21** (1986) 2224.
23. S. M. L. SASTRY, T. C. PENG and R. J. LEDERICH, in "Mechanical Behaviour of Rapidly Solidified Materials", edited by S. M. L. Sastry and B. A. MacDonald, (The Metalurgical Society of AIME, Warrendale, PA 1986) p. 207.
24. Z. FAN, P. TSAKIROPOULOS and A. P. MIODOWNIK, *Mater. Sci. Tech.* **8** (1992) 922.
25. C. R. BROOKS (ed.), "Heat Treatment, Structure and Properties of Nonferrous Alloys" (ASM, Metals Parks, Ohio, USA, 1982) p. 329.
26. L. CHANDRASEKARAN, unpublished research work (1992).
27. A. I. KAHVECI and G. E. WELSCH, *Scripta Metall.* **20** (1986) 1287.
28. J. MURRAY (ed.), "Phase Diagrams of Binary Titanium Alloys" (ASM, Metals Park, Ohio, USA, 1987) p. 33.
29. Z. FAN, PhD thesis, University of Surrey, Guildford, UK (1993).
30. G. V. SAMSONOV and Y. S. UMANSKIY, "Hard Compounds of Refractory Metals", Technical Translation TT-F-12, National Aeronautics and Space Administration, June 1962.
31. Y. T. LEE, M. PETERS and G. WELSCH, *Met. Trans.* **22A** (1991) 709.
32. T. SAITO and T. FURUTA, private communication (1992).
33. Z. FAN, A. P. MIODOWNIK and P. TSAKIROPOULOS, *Mater. Sci. Technol.*, in press.
34. O. B. PEDERSEN, *ZAMM* **58** (1978) 227.
35. O. B. PEDERSEN, *Acta Metall.* **31** (1983) 1795.
36. A. P. MIODOWNIK, private communication (1992).
37. S. M. LANG, "Properties of High Temperature Ceramics and Cermets: Elasticity and Density at Room Temperature", NBS Monograph 6, 1, March 1960 (National Bureau of Standards, Washington, DC, 1960).

Received 16 August
and accepted 14 September 1993